CHEMISTRY
A EUROPEAN JOURNAL

DOI: 10.1002/chem.200901628

Universal Features of the Electron Density Distribution in Hydrogen-Bonding Regions: A Comprehensive Study Involving H···X (X = H, C, N, O, F, S, Cl, π) Interactions

Ignasi Mata,[a] Ibon Alkorta,[b] Elies Molins,[a] and Enrique Espinosa*[c]

Abstract: Topological analyses of the theoretically calculated electron densities for a large set of 163 hydrogen-bonded complexes show that H···X interactions can be classified in families according to X (X = atom or π orbital). Each family is characterised by a set of intrinsic dependencies between the topological and energetic properties of the electron density at the hydrogen-bond critical point, as well as between each of them and the bonding distance. Comparing different atom-acceptor families, these dependencies are classified as a function of the van der Waals radius r_X or the electronegativity χ_X, which can be explained in terms of the molecular orbitals involved in the interaction. According to this ordering, the increase of χ_X leads to a larger range of H···X distances for which the interaction is of pure closed-shell type. Same dependencies observed for H···O interactions experimentally characterised by means of high-resolution X-ray diffraction data show a good agreement with those obtained from theoretical calculations, in spite of a larger dispersion of values around the expected fitting functions in the experimental case. Theoretical dependencies can thus be applied to the analysis of the experimental electron density for detecting either unconventional hydrogen bonds or problems in the modelling of the experimental electron density.

Keywords: Bond theory · electron density · hydrogen bonds · topology

Introduction

The topological analysis of the electron density distribution $\rho(\mathbf{r})$, performed in the framework of the quantum theory of atoms in molecules (QTAIM),[1] is extensively used for the study of all kinds of interatomic interactions.[2] According to QTAIM, any bonding interaction between atoms exhibits a $\rho(\mathbf{r})$ saddle topology in the internuclear region, and the concomitant bond critical point (BCP) at the interatomic surface S, as a consequence of the bond path formation. The bond path connects the nuclei and is defined as the trajectory where $\rho(\mathbf{r})$ is a maximum with respect to any neighboring line linking the nuclei. The bond path is thus formed by two gradient lines $\nabla\rho(\mathbf{r})$ starting at the BCP and ending at the nuclear positions. At the BCP, $\rho(\mathbf{r})$ is a minimum along the bond path and a maximum in the perpendicular plane, therefore leading to $\nabla\rho(\mathbf{r}) = 0$. Hence, the BCP appears at the intersection of the bond path with S, which behaves as a zero-flux surface of $\rho(\mathbf{r})$ (i.e., S is not crossed by any gradient line: $\nabla\rho(\mathbf{r})\cdot\mathbf{n}(\mathbf{r}) = 0\ \forall\mathbf{r} \in S$, $\mathbf{n}$ being the unit vector perpendicular to S at $\mathbf{r}$). The bond path and the concomitant BCP at S have been proposed as universal indicators of bonded interactions.[3]

Electron properties at the BCP are extensively used for the characterisation of interatomic interactions from the electron density distribution,[4] which can be theoretically calculated from quantum wavefunctions[5] or experimentally determined from single crystal X-ray diffraction.[6] Commonly reported properties of $\rho(\mathbf{r})$ at the BCP are: i) the total electron density (ρ), ii) the three main curvatures (λ_i, $i = 1, 2, 3$) that correspond to the eigenvalues of the Hessian matrix $\partial^2\rho/\partial x_i\partial x_j$ (λ_3 is positive and associated to the bond path direction, and λ_1 and λ_2 are negative and associated to

[a] Dr. I. Mata, Prof. E. Molins
Institut de Ciència de Materials de Barcelona (ICMAB-CSIC)
Campus UAB, 08193 Bellaterra (Spain)

[b] Prof. I. Alkorta
Instituto de Química Médica (IQM-CSIC)
Juan de la Cierva, 3, 28006 Madrid (Spain)

[c] Prof. E. Espinosa
Laboratoire de Cristallographie
Résonance Magnétique et Modélisations
CRM²(UMR CNRS 7036), Nancy-Université, Faculté des Sciences
BP 239, 54506 Vandoeuvre-lès-Nancy (France)
Fax: (+33) 383-40-6492
E-mail: Enrique.espinosa@crm2.uhp-nancy.fr

Supporting information for this article is available on the WWW under http://dx.doi.org/10.1002/chem.200901628.

two directions parallel to S), iii) the Laplacian $\nabla^2\rho = \Sigma_i \lambda_i$ (it indicates the regions where $\rho(\mathbf{r})$ is locally concentrated $\nabla^2\rho < 0$, or depleted $\nabla^2\rho > 0$) and iv) the local electron kinetic, potential and total energy densities ($G > 0$, $V < 0$ and $H = G + V$, respectively). Hereafter, (i) to (iii) and (iv) will be respectively referred as the topological and the energetic properties of $\rho(\mathbf{r})$ at the BCP. It should be noted that while the former can be experimentally determined from high-resolution X-ray diffraction data, the latter are not straightforwardly accessible from experiments.

Closed shell interactions, such as hydrogen bonds (HB), are recognised in the topology of $\rho(\mathbf{r})$ by a positive Laplacian at the BCP ($\nabla^2\rho > 0$). In this case, the energetic properties can be estimated from the experimental $\rho(\mathbf{r})$ by using the Abramov functional of the kinetic energy density,[7] which is based on the semi-classical Thomas–Fermi equation[8] with gradient quantum corrections,[9,10] and the local form of the virial theorem.[11] This method was applied for the first time to a large set of 83 experimentally determined X–H···O (X = O, N, C) hydrogen bonds[12] and its validity tested against a set of 32 theoretically calculated X–H···F–Y interactions.[13]

Dependencies between topological properties and bonding distances were first observed for HBs,[14] and after for other interactions,[15] by means of theoretical calculations on molecules and complexes in gas phase. Since then, many dependencies involving $\rho(\mathbf{r})$ properties at the BCP have been reported and used in theoretical analyses of complexes in the gas phase, such as those given in the detailed study of N–H···N interactions.[16,17] Similar dependencies for HBs have been observed in crystals from experimental electron density distributions determined by using high-resolution X-ray diffraction data[12,18–20] of from theoretical calculations.[21]

In the analysis of these dependencies, typically through least squares fits, the values of the properties at the BCP present some degree of dispersion around the fitting curves. When using experimental data, this dispersion is usually attributed to observational errors, which correspond to the difference between the experimentally determined and the exact magnitude of $\rho(\mathbf{r})$ and affect the derived topological and energetic properties at BCP. These errors can be important because of the difficult modelling of the electron distribution in the intermolecular regions, where $\rho(\mathbf{r})$ is flatter than within molecules and the relevance of the experimental noise is relatively more important. On the other hand, theoretical calculations of properties at BCP carried out on large families of complexes presenting H···F and H···N HBs strongly suggest that deviations from the expected dependencies are also related to the effect of the environment on the atoms directly involved in the interaction.[22,23] However, as far as this dispersion is small enough, the set of dependencies associated to these families of complexes appears well defined. Accordingly, the set of dependencies obtained for a given family can be taken as fundamental descriptors of the interaction, and can be used for its characterisation, independently of the individual systems used for the derivation of the dependencies.

It has been shown that these dependencies are a consequence of the electronic shell structure of the atoms, their existence being hence a universal trait of the interatomic interaction.[24] Herein, the case of HBs is studied in detail through theoretical calculations carried out for a large set of 163 hydrogen-bonded complexes, revealing that H···X HBs can be classified in families depending on the acceptor entity X (X = atom or π system, see Table 1).

Table 1. Distribution of the 163 hydrogen-bonded complexes in families of n members according to the acceptor X.

X	n
H	30
C	15
N	20
O	24
F	19
S	20
Cl	20
π	15

The complexes belonging to the family X = H correspond to DH···HA interactions, with D = C, N and A = Li, Na, Be, Mg. In these complexes, H(−A) presents a negative charge due to the electropositive character of A. Thus, the reported H···H interactions correspond to dihydrogen bonds,[25] where one of the hydrogen atoms acts as donor and the other as acceptor. This kind of hydrogen bonding should be distinguished from a van der Waals interaction between two similarly charged hydrogen atoms,[26] not included in this study.

When the acceptor is an atom, these dependencies can be classified with atomic properties like the van der Waals radius r_X or the electronegativity χ_X. The theoretical dependencies presented here validate those derived from X-ray diffraction data, and can be useful in the analysis of the experimental electron density.

Results and Discussion

Dependencies of the electron density properties at the BCP with the hydrogen bond distance: The values of ρ, λ_3, $|\lambda_1 + \lambda_2|$, G and $|V|$ for all calculated complexes are represented against d_{HB} in Figure 1. Log-linear plots were preferred to underline the exponential behaviours observed for each family. For a given distance, the magnitude of the property, as seen from the represented fitting functions, increases along the series H < F < O < N < C < Cl < S, following the van der Waals radius (r_X) of these atoms (1.20 < 1.47 < 1.52 < 1.55 < 1.70 < 1.75 < 1.80 Å).[27] This classification can be observed in Figure 2 for ρ, λ_3 and $|\lambda_1 + \lambda_2|$.

A HB picture arising from the topology of $\rho(\mathbf{r})$ suggests that properties at the BCP are governed by both the repulsion between the closed shells of the hydrogen and the acceptor atoms, dominated by the requirements of the Pauli exclusion principle, and by the stabilizing effect of the elec-

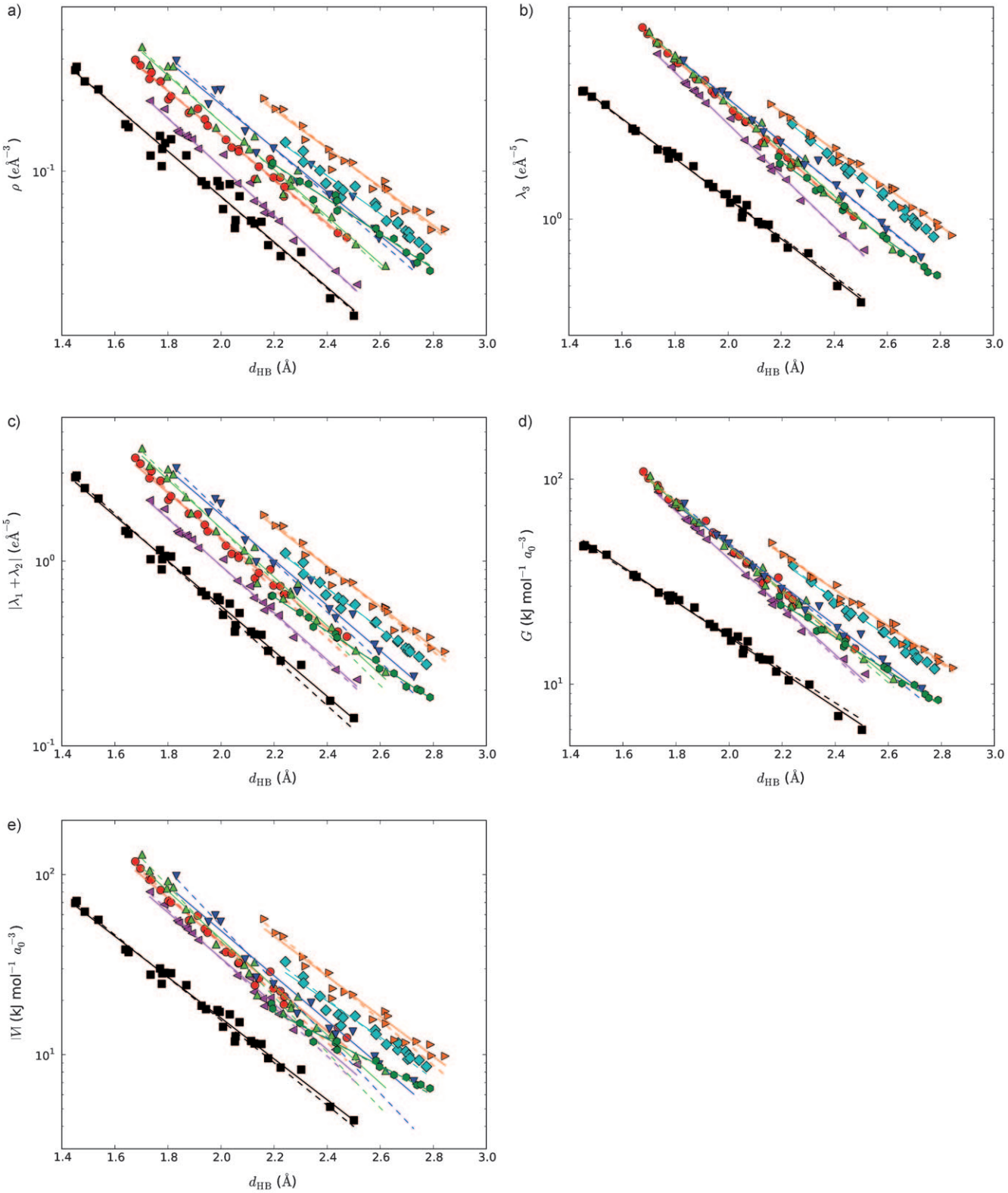

Figure 1. a) ρ, b) λ_3, c) $|\lambda_1 + \lambda_2|$, d) G, e) $|V|$ versus d_{HB}. For these properties, the families are classified along the series X = H, F, O, N, C, Cl and S (X = π being a particular case, see text) and they are respectively represented by the coloured symbols: black squares, magenta left-triangles, red circles, green up-triangles, blue down-triangles, cyan diamonds, orange right-triangles and dark green hexagons. Solid lines are the linear regressions on linearised data given in Table 2. Dashed lines stand for least squares fits against the original (non-linearised) data.

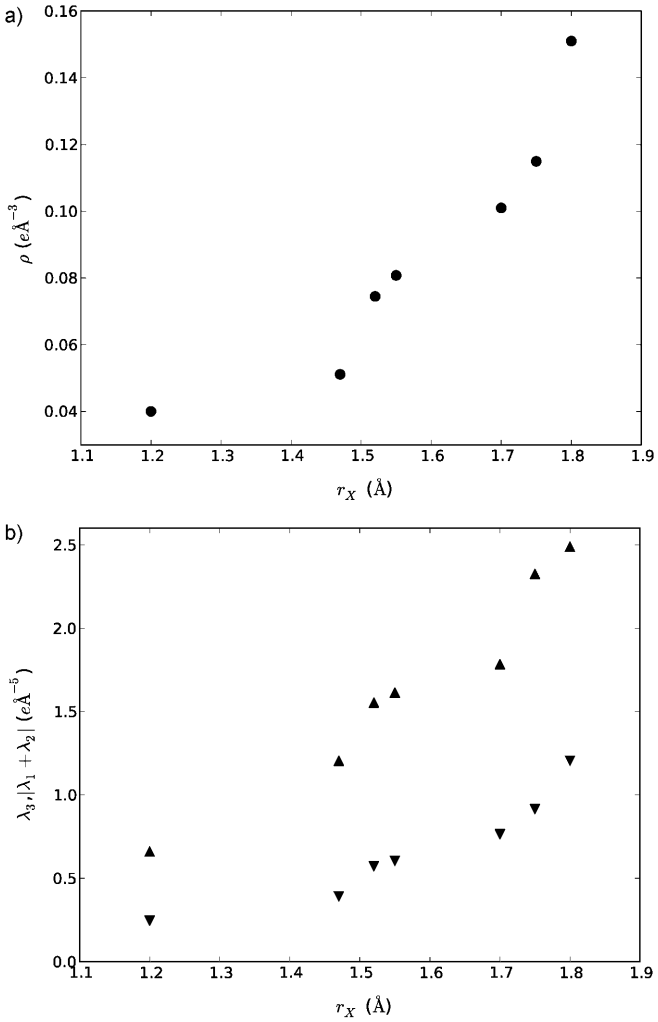

Figure 2. a) ρ and b) λ_3 (▲) and $|\lambda_1 + \lambda_2|$ (▼) versus van der Waals radius of X in H···X at d_{HB} = 2.3 Å. Topological values have been interpolated from the fits given in Table 2 (solid lines in Figure 1).

tric field on the H···X region, dominated by the H-nucleus contribution.[23] An important parameter in this description of hydrogen bonding is the mutual penetration of the closed shells,[28] which can be quantified by the difference between the sum of the van de Waals radii of the interacting atoms and the HB distance.

For a given d_{HB}, the increase of r_X leads to a larger penetration of the H···X closed shells. This effect is similar to that observed when shortening the hydrogen bond distance and, therefore, the same interpretation given for the exponential dependencies of ρ, λ_3, $|\lambda_1 + \lambda_2|$, G and $|V|$ with d_{HB} can be applied, to a first approximation, to the variations with r_X at the same H···X distance. Hence, the larger the penetration the higher value of the electron density (larger ρ) and the stronger repulsion (larger G) in the bonding region, meaning that $\rho(\mathbf{r})$ is steeper in this region (larger λ_3). Moreover, as the hydrogen atom is depopulated by the polarisation of its electron density towards the donor D,[29] the hydrogen nucleus follows a partial de-screening, leading to an increase of its associated electric field that pushes the electron density toward the bond axis[23] (larger $|\lambda_1 + \lambda_2|$), with the concomitant stabilisation of the electron density (larger $|V|$). According to this view, λ_3 and G appear related to the closed-shell repulsion, while $|\lambda_1 + \lambda_2|$ and $|V|$ show the effect of the electric field in the internuclear region.[23]

However, it should be noted that there is an important difference between the r_X variation at a fixed d_{HB} distance and the d_{HB} variation for a given r_X radius. Indeed, this is indicated by the grouping of families according to the row of the acceptor atom in the periodic table (i.e., as a function of the number of shells of this atom). This trend shows in the exponential dependencies of Figure 1, in particular for λ_3 and G, where it is observed the grouping of the fitting functions by the period of the acceptor atom.

The grouping of the exponential dependencies by the acceptor atom properties (r_X and period) explains the behaviour of $\nabla^2\rho$ and H (Figure 3). The dependency of these two properties with d_{HB} shows a more complex form than a simple exponential, reflecting qualitative changes of the molecular orbitals involved in the hydrogen bond.[22,30] Thus, at long hydrogen bond distances, both properties are positive and increase slowly as d_{HB} is reduced until a maximum is reached, then drop quickly to negative values. As H is bounded by the condition $H < \nabla^2\rho$,[31] three regions can be established according to the signs of both properties.[22] They correspond to i) shared interactions (short d_{HB}, $\nabla^2\rho < 0$ and $H < 0$), ii) pure closed-shell interactions (long d_{HB}, $\nabla^2\rho > 0$ and $H > 0$) and iii) closed-shell interactions of intermediate character that belong to a transition region between the two former and are associated to distances in the range $d_{HB}(\nabla^2\rho=0) < d_{HB} < d_{HB}(H=0)$.[22]

According to this interpretation, HBs in the calculated complexes fall in the pure closed shell and transition regions, being all interactions of closed shell type ($\nabla^2\rho > 0$). The transition region deserves special attention as it has been seen that most of the molecular orbital reorganisation related to the transformation of the interaction from pure closed- to shared-shell takes place here.[22] HBs belonging to the intermediate region present a significant shared character, which makes them stronger than those of pure closed-shell type. $H < 0$ is also observed in other closed-shell interactions where the orbitals of the interacting entities are significantly perturbed as a result of the interaction. This is the case of metal–metal[32] or metal–ligand bonds .[33]

To model the behaviours of $\nabla^2\rho$ and H with d_{HB} in the whole range of interaction distances, their dependencies have been fitted to functions containing exponential terms.[20,22,30] For closed shell interactions, the $\nabla^2\rho$ dependency can be approximated to an exponential for all families but H···H (Table 2), as in this last case the effect of the transition to a shared interaction appears for shorter d_{HB} distances. The corresponding data, represented in Figure 3, have not been fitted. Instead of this, plotted lines are calculated from the exponential dependencies given in Figure 1 for λ_3,

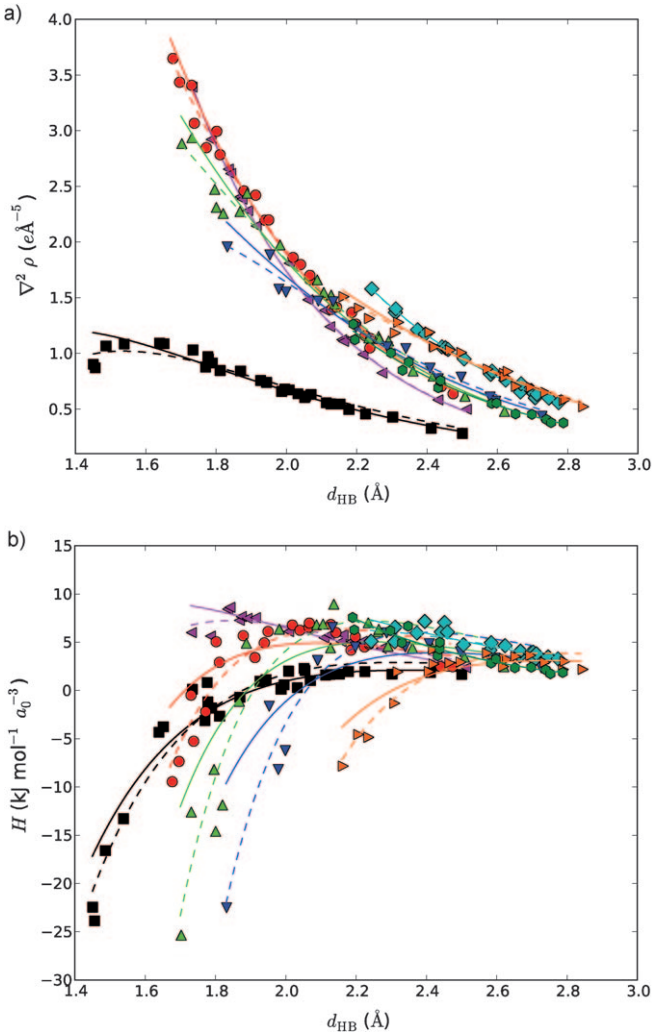

Figure 3. a) $\nabla^2\rho$ and b) H versus d_{HB}. Plotted lines have been calculated from the linear regressions on linearised data (solid) or from exponential fittings (dashed) carried out for data depicted in Figure 1 (see Table 1) and by using the correspondences $\nabla^2\rho = \Sigma\lambda_i$ and $H = G + V$. Colours and symbols are defined as in Figure 1.

$|\lambda_1 + \lambda_2|$, G and $|V|$. Using the least squares method, an apparently better agreement is observed for exponential than for linear fittings, feature which is related to the bias toward higher values that is observed in the first case. However, these differences are not relevant as they do not affect the classification pointed for the calculated dependencies.

The dependencies of $\nabla^2\rho$ and H with d_{HB} are grouped for acceptor atoms belonging to the same row of the periodic table, appearing an ordering with the atomic number Z inside each row (equivalent to a classification with r_X) that is analogous to that observed on the behaviour of λ_3 versus d_{HB} and G versus d_{HB}. This is clearer for $\nabla^2\rho$, where data belonging to different rows or periods are neatly separated, than for H, where they appear superposed. The ordering inside each period suggests that the transition from a closed shell to a shared interaction is favoured as r_X increases. Indeed, this is clearly shown by the shift of $H = 0$ to larger distances with r_X, indicating that the transition region extends to longer d_{HB}. For each period, the $\nabla^2\rho$ dependencies with d_{HB} appear grouped and superposed, making the classification unclear in a wide range of distances. However, it can be seen that at long d_{HB} the Laplacian value increases with r_X, while at short d_{HB} values the slope of the curve decreases with r_X. Whereas the behaviour at long d_{HB} values is explained by the penetration of the closed shells within the H···X region (in the same terms as previously pointed for the exponential properties), that at short d_{HB} values suggests that the $\nabla^2\rho$ maximum, which is outside the range of d_{HB} distances considered here, moves to larger d_{HB} with r_X. This feature also indicates that the transition to a shared interaction takes place at longer d_{HB} when r_X increases.

There are several effects that can contribute to the shift of the transition region with r_X within a period. A larger r_X value means that the penetration will increase faster when approaching the H-bonded molecules, thus favouring the transition to a shared interaction at longer distances. Moreover, the observed dependencies for a given period are not ordered by r_X only but also by other atomic properties, such as electronegativity (χ_X) or the number of electrons in the valence shell ($n_{val,X}$), both of them increasing as r_X decreases. Given the increased shared character and the concomitant dative nature of the bonding interaction that appears when two hydrogen bonded molecules approach to each other, a larger χ_X of the acceptor atom leads to a more difficult formation of the H···X bonding molecular orbital, and the transition starts hence at shorter distances. Moreover, it has been shown that electrons belonging to the valence shell but not being involved in the hydrogen bond hinder the transition towards a shared interaction,[34] $n_{val,X}$ having therefore an effect analogous to χ_X in the transition.

Among the H···X families treated in this work, H···π shows up as a particular case. This feature is clearly related to the fact that here the HB interaction involves a delocalised molecular orbital as acceptor. The calculated fitting functions for the H···π dependencies cross those of several families belonging to the second period. It should be noted however that H···π data are plotted against the distance between H and the bond critical point associated to the π system. As expected, all H···π interactions are of pure closed shell type[22] and no evidence of transition to shared interaction is observed. Even with this particularity, it is noteworthy that the H··· π family follows the same kind of dependencies than any other analysed here, in spite the hydrogen does not interact with electrons belonging to a unique atom. In this way, the observed dependencies between the topological and energetic properties with d_{HB} are not only universal for interatomic interactions, as previously pointed out,[24] but they also appear in intermolecular interactions involving molecular orbitals that are delocalised over several atoms.

Dependencies between the electron density properties at BCP: The dependencies $|\lambda_1 + \lambda_2|$ versus λ_3 and $|V|$ versus G are shown in Figure 4a and 4b for all H···X families. Both

Table 2. Fitting parameters a and b, root mean square deviations (RMSD), normalised RMSD (NRMSD) and correlation coefficient (R^2) for all linear regressions. R^2 in first column has been calculated with data from the eight families. Values in column X=O (Exp) have been calculated from experimental data taken from references [12, 18, 19].

	X = H	X = F	X = O	X = N	X = C	X = Cl	X = S	X = π	X=O (Exp)
$\ln(y)=\ln(a)\ -b\cdot x$									
λ_3 vs. d_{HB}									
$\ln(a)$	4.36(6)	6.31(9)	6.04(6)	6.03(9)	5.68(13)	5.82(9)	5.5(1)	5.08(8)	5.93(14)
a	79(4)	550(46)	421(25)	415(39)	294(38)	335(30)	232(26)	161(13)	375(53)
b	2.08(3)	2.66(4)	2.44(3)	2.41(5)	2.22(6)	2.16(4)	1.97(4)	2.04(2)	2.33(7)
RMSD	0.041	0.038	0.032	0.052	0.057	0.025	0.039	0.025	0.169
NRMSD	0.019	0.019	0.017	0.023	0.028	0.022	0.029	0.020	0.051
$R^2=0.9963$	0.9949	0.9960	0.9967	0.9939	0.9915	0.9952	0.9913	0.9966	0.9305
$\lvert\lambda_1+\lambda_2\rvert$ vs. d_{HB}									
$\ln(a)$	5.1(1)	5.8(1)	5.9(1)	6.5(2)	6.2(3)	5.7(2)	6.0(2)	4.3(1)	5.7(3)
a	158(18)	332(43)	378(51)	650(140)	510(140)	295(53)	396(85)	71(7)	269(95)
b	2.81(6)	2.93(6)	2.82(7)	3.03(14)	2.83(12)	2.51(7)	2.52(9)	2.14(4)	2.77(16)
RMSD	0.086	0.058	0.072	0.119	0.119	0.051	0.077	0.030	0.385
NRMSD	0.028	0.026	0.032	0.043	0.046	0.037	0.045	0.024	0.078
$R^2=0.9891$	0.9879	0.9922	0.9881	0.9804	0.9778	0.9859	0.9798	0.9955	0.7856
ρ vs. d_{HB}									
$\ln(a)$	1.9(2)	2.5(1)	2.4(1)	2.8(2)	2.6(2)	2.1(2)	2.5(2)	1.5(2)	2.0(2)
a	6.6(10)	12.1(15)	10.7(13)	16.1(32)	13.9(34)	8.2(15)	11.7(26)	4.5(8)	7.6(18)
b	2.22(8)	2.38(6)	2.16(6)	2.30(9)	2.1(1)	1.85(7)	1.89(9)	1.70(7)	2.05(12)
RMSD	0.110	0.057	0.063	0.109	0.108	0.053	0.079	0.050	0.286
NRMSD	0.045	0.032	0.036	0.051	0.054	0.051	0.061	0.047	0.087
$R^2=0.9790$	0.9692	0.9887	0.9846	0.9716	0.9685	0.9724	0.9630	0.9810	0.7853
$\nabla^2\rho$ vs. d_{HB}									
$\ln(a)$	2.0(2)	5.59(7)	4.92(9)	4.4(2)	3.9(2)	4.84(9)	3.7(1)	4.5(2)	5.1(2)
a	7(1)	267(19)	138(12)	80(12)	48(9)	127(12)	42(6)	92(14)	164(27)
b	1.21(9)	2.52(4)	2.15(4)	1.90(7)	1.68(8)	1.96(4)	1.52(6)	1.98(6)	2.14(8)
RMSD	0.129	0.032	0.046	0.081	0.081	0.026	0.051	0.046	0.197
NRMSD	0.095	0.017	0.027	0.045	0.054	0.025	0.048	0.038	0.069
$R^2=0.9838$	0.8725	0.9968	0.9914	0.9769	0.9714	0.9937	0.9753	0.9878	0.8921
G vs. d_{HB}									
$\ln(a)$	6.78(6)	9.1(1)	8.79(8)	8.8(1)	8.4(1)	8.3(1)	8.2(2)	7.4(1)	8.8(1)
a	$0.88(5)10^3$	$8.8(9)10^3$	$6.6(6)10^3$	$6.4(6)10^3$	$4.3(6)10^3$	$3.9(5)10^3$	$3.6(6)10^3$	$1.6(2)10^3$	$6.5(9)10^3$
b	1.97(3)	2.69(5)	2.47(4)	2.46(5)	2.26(6)	2.09(5)	2.01(6)	1.89(5)	2.40(7)
RMSD	0.046	0.048	0.045	0.053	0.061	0.036	0.054	0.035	0.165
NRMSD	0.022	0.024	0.023	0.023	0.029	0.031	0.039	0.030	0.049
$R^2=0.9949$	0.9929	0.9937	0.9939	0.9941	0.9909	0.9896	0.9842	0.9921	0.9377
$\lvert V\rvert$ vs. d_{HB}									
$\ln(a)$	8.0(1)	9.4(2)	9.4(2)	9.9(3)	9.6(3)	8.5(3)	9.5(3)	6.6(2)	9.3(2)
a	$3.0(3)10^3$	$11.8(21)10^3$	$12.4(21)10^3$	$20.2(50)10^3$	$15.4(50)10^3$	$5.0(14)10^3$	$12.8(38)10^3$	$0.8(1)10^3$	$10.8(2)10^3$
b	2.62(6)	2.92(8)	2.84(8)	3.07(12)	2.88(14)	2.31(11)	2.56(12)	1.72(7)	2.77(10)
RMSD	0.083	0.078	0.090	0.137	0.145	0.080	0.106	0.055	0.236
NRMSD	0.030	0.035	0.040	0.049	0.055	0.060	0.060	0.051	0.057
$R^2=0.9842$	0.9871	0.9860	0.9819	0.9748	0.9688	0.9593	0.9633	0.9771	0.907
$\ln(y)=\ln(a)-b\cdot\ln(x)$									
$\lvert\lambda_1+\lambda_2\rvert$ vs. λ_3									
$\ln(a)$	−0.85(1)	−1.15(1)	−1.07(3)	−1.11(3)	−1.01(3)	−1.07(1)	−0.98(2)	−1.07(1)	−1.40(8)
a	0.429(5)	0.318(3)	0.343(9)	0.331(11)	0.364(10)	0.343(4)	0.375(6)	0.342(4)	0.248(19)
b	1.36(2)	1.10(1)	1.16(2)	1.26(3)	1.28(3)	1.16(2)	1.28(3)	1.05(3)	1.21(5)
RMSD	0.052	0.026	0.053	0.080	0.071	0.035	0.049	0.047	0.291
NRMSD	0.017	0.011	0.024	0.029	0.027	0.025	0.029	0.037	0.059
$R^2=0.9953$	0.9956	0.9958	0.9935	0.9910	0.9920	0.9934	0.9918	0.9894	0.8779
$\lvert V\rvert$ vs. G									
$\ln(a)$	−0.98(6)	−0.51(4)	−0.70(7)	−1.04(12)	−1.06(13)	−0.62(9)	−1.00(9)	−0.07(9)	−0.81(10)
a	0.37(2)	0.60(3)	0.50(4)	0.35(4)	0.35(4)	0.54(5)	0.37(3)	0.93(8)	0.44(5)
b	1.33(2)	1.09(1)	1.16(2)	1.25(3)	1.28(4)	1.11(3)	1.28(3)	0.91(3)	1.15(3)
RMSD	0.057	0.030	0.052	0.091	0.088	0.048	0.053	0.047	0.148
NRMSD	0.020	0.014	0.023	0.033	0.033	0.036	0.030	0.043	0.036
$R^2=0.9941$	0.9939	0.9979	0.9939	0.9888	0.9885	0.9855	0.9907	0.9838	0.9631
$y=a\ +\ b\cdot x$									
G vs. λ_3									
a	1.5(2)	−0.9(3)	−1.2(5)	−1.9(6)	−1.7(7)	0.3(3)	−1.1(5)	0.9(2)	−3.0(16)
b	12.5(2)	15.6(1)	14.9(1)	14.8(2)	14.5(3)	13.7(2)	14.7(2)	13.3(2)	15.8(3)
RMSD	0.551	0.569	1.002	1.373	1.365	0.425	0.759	0.312	6.054
NRMSD	0.013	0.008	0.011	0.015	0.021	0.016	0.021	0.017	0.032

Table 2. (Continued)

	X = H	X = F	X = O	X = N	X = C	X = Cl	X = S	X = π	X=O (Exp)
$R^2=0.9986$	0.9979	0.9994	0.9987	0.9977	0.9952	0.9969	0.9952	0.9974	0.9714
V vs. $\lvert\lambda_1+\lambda_2\rvert$									
a	2.1(2)	−0.8(6)	−0.7(4)	−2.2(10)	−2.6(11)	0.46(5)	−1.3(7)	1.7(4)	4.2(25)
b	24.3(2)	37.4(6)	32.2(5)	31.1(5)	30.1(8)	27.6(8)	30.8(8)	25.1(10)	33.4(12)
RMSD	0.751	1.278	2.151	2.622	2.578	0.845	1.474	0.616	12.347
NRMSD	0.011	0.018	0.020	0.022	0.028	0.035	0.031	0.048	0.047
$R^2=0.9960$	0.9984	0.9964	0.9955	0.9951	0.9907	0.9848	0.9889	0.9783	0.9055
$\lvert V\rvert/G$ vs. $\lvert\lambda_1+\lambda_2\rvert/\lambda_3$									
a	0.113(7)	0.146(90)	0.048(41)	−0.016(30)	−0.063(45)	0.173(82)	−0.017(48)	0.54(22)	0.389(30)
b	1.79(1)	1.97(26)	2.06(10)	2.11(7)	2.13(10)	1.59(23)	2.11(11)	0.56(65)	1.26(8)
RMSD	0.008	0.025	0.021	0.025	0.032	0.025	0.027	0.041	0.076
NRMSD	0.011	0.144	0.069	0.047	0.056	0.128	0.068	0.257	0.098
$R^2=0.9767$	0.9983	0.7734	0.9513	0.9814	0.9719	0.7327	0.9527	0.0552	0.7503
ρ vs. λ_3									
a	−0.010(3)	0.010(2)	0.015(3)	0.002(5)	−0.001(5)	0.010(2)	0.000(3)	0.012(3)	0.001(9)
b	0.0715(18)	0.0349(6)	0.0390(7)	0.0480(15)	0.0568(20)	0.0453(13)	0.0614(16)	0.0518(30)	0.0352(18)
RMSD	0.009	0.004	0.006	0.012	0.010	0.003	0.005	0.005	0.036
NRMSD	0.035	0.022	0.024	0.040	0.039	0.037	0.034	0.069	0.07
$R^2=0.9890$	0.9833	0.9946	0.9938	0.9838	0.9834	0.9845	0.9881	0.9592	0.8247

sets of dependencies exhibit the same classification than that observed for H and $\nabla^2\rho$ (i.e., the families can be grouped according to the period of X, being then ordered by r_X within the same group). These dependencies show the balance between the aforementioned effects of closed shell repulsion and electric field stabilisation. As seen in Figure 4a and 4b, the slopes increase with r_X along each group, indicating that $|\lambda_1 + \lambda_2|$ and $|V|$, related to the stabilizing effect of the electric field, become more important as the values of these properties increase, or similarly as the bonding distance shortens. This agrees with the shift of the transition region to larger d_{HB} with r_X because the stabilisation of a higher quantity of charge induced by the electric field favours the shared character of the interaction.

A similar classification of the families is also observed for the linear dependencies between the curvatures and the energetic properties (G vs. λ_3 and $|V|$ vs. $|\lambda_1 + \lambda_2|$, given in Figure 4c and 4d, respectively) and in the dependency λ_3 versus ρ (Figure 4e). In the case of G versus λ_3 the separation is so small that a single linear function could be fitted for all families ($G=14.80(9)\ \lambda_3-1.2(2)$, $R^2=0.994$, RMSD = 1.74, NRMSD = 0.017, $n=163$), indicating that this dependency is mostly independent of χ_X, r_X and $n_{val,X}$, as well as of the molecular environment around the H···X interaction, in particular for weaker interactions, where G and λ_3 exhibit lower values. This feature seems particularly interesting because it could be used to detect problems in the modelling of $\rho(\mathbf{r})$, either experimentally determined or theoretically calculated, if significant outliers with respect to the fitting function appear.

The dependency $|V|/G$ versus $|\lambda_1 + \lambda_2|/\lambda_3$ is shown in Figure 4f. According to the local form of the virial theorem ($2G + V = \frac{1}{4}\nabla^2\rho$, in a.u.)[1] and to the definition of H, the limits of the transition region, $\nabla^2\rho=0$ and $H=0$, can be respectively expressed as $|V|/G=2$ and $|V|/G=1$ and, therefore, the internuclear distances corresponding to $|V|/G<1$, $1<|V|/G<2$ and $2<|V|/G$ indicate interactions of pure closed-shell, transition and shared type, respectively. When $|V|/G$ is plotted against $|\lambda_1 + \lambda_2|/\lambda_3$, the well established linear behaviours between curvatures and energy densities lead to a linear dependency between both ratios that exhibits a slope close to 2 (Table 2) except for X=π. While the slope remains roughly similar for any X=H, C, N, O, F, S or Cl, the $|V|/G$ ratio increases with r_X along the families for which X belongs to the same period, again indicating that a higher van der Waals radius favours the concentration of electrons and therefore a starting shared character of the interaction.

As previously observed for the H···π dependencies with d_{HB}, here this family behaves qualitatively as the others, as shown in Figure 4a to 4e. According to the observed features in these figures, there is no formal distinction between this kind of interaction and conventional HBs. The only significant difference appears in the case $|V|/G$ versus $|\lambda_1 + \lambda_2|/\lambda_3$, for which H···π does not present a clear dependence, as the other families do (while the fitting parameter b exhibits a very large error, the RMSD and NRMSD values are much larger than those of the other families, as shown in Table 2). This trend can be explained from the small range of $|\lambda_1 + \lambda_2|/\lambda_3$ values in this case, meaning that the balance between $|\lambda_1 + \lambda_2|$ and λ_3 tends to remain constant as d_{HB} varies. That is not surprising, as this ratio is indicative of the balance between the closed shell/shared character of the interaction, which should not vary significantly in the H···π case, as this interaction is expected to remain as pure closed shell in the whole range of possible interaction distances.

Experimental against theoretical dependencies: Most of the dependencies calculated from experimental data for H···O hydrogen bonds (X=O (Exp) in Table 2) are very similar to those theoretically calculated for the H···O family. The agreement is very good for the exponential dependencies with d_{HB} (see Figure 5a for the cases λ_3 and $|\lambda_1 + \lambda_2|$), being most of the a and b parameters calculated from exper-

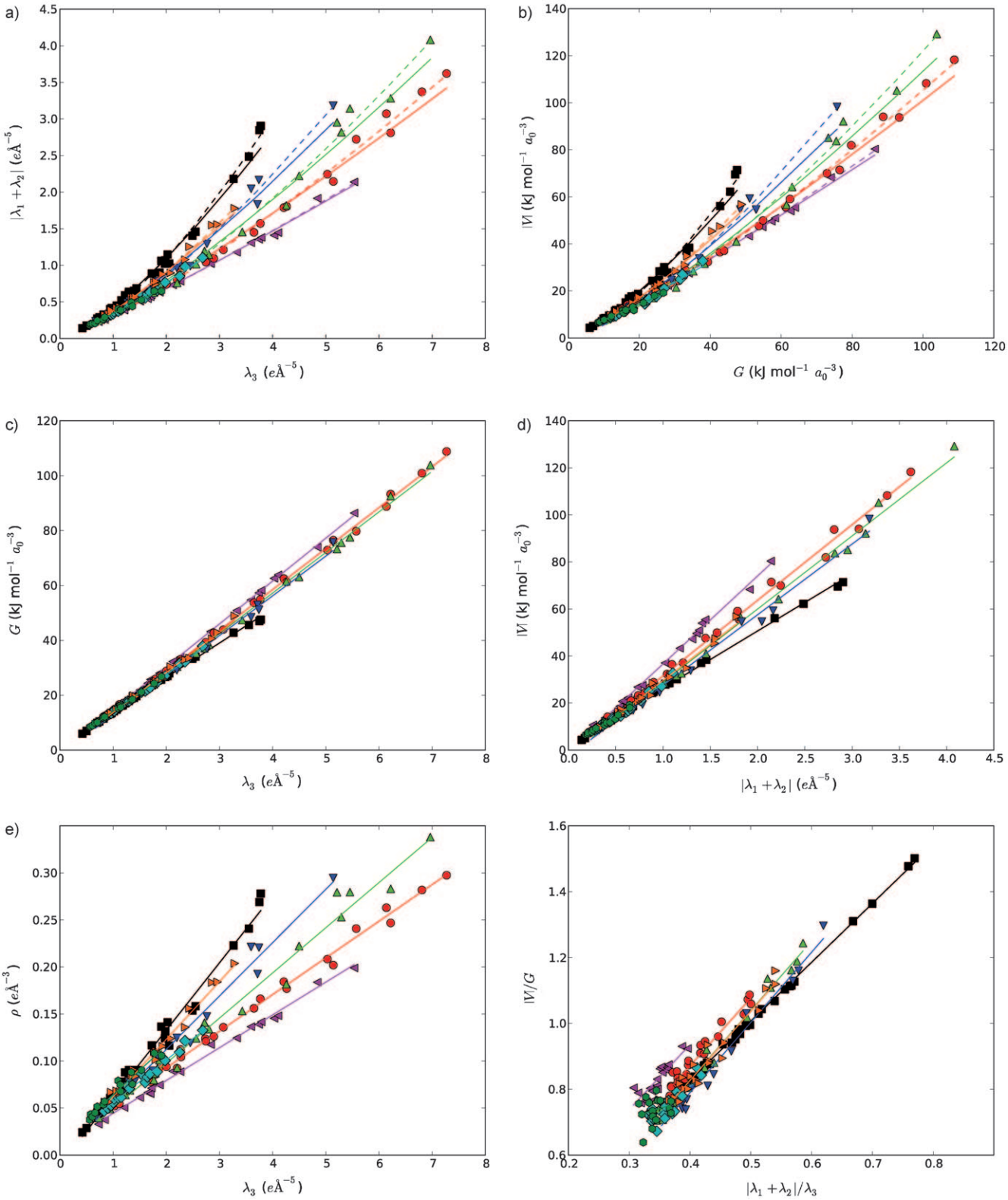

Figure 4. a) $|\lambda_1 + \lambda_2|$ versus λ_3, b) $|V|$ versus G, c) G versus λ_3, d) $|V|$ versus $|\lambda_1 + \lambda_2|$, e) ρ versus λ_3, f) $|V|/G$ versus $|\lambda_1 + \lambda_2|/\lambda_3$. Colours and lines are defined as in Figure 1.

imental and theoretical data equal within standard uncertainties. Theoretical $\nabla^2\rho$ versus d_{HB} and H versus d_{HB} dependencies provide a fair approximation to the experimental ones (Figure 5b and 5c), in spite some systematic deviations are observed. This is particularly cumbersome in Figure 5c, where the large dispersion of experimental values makes the

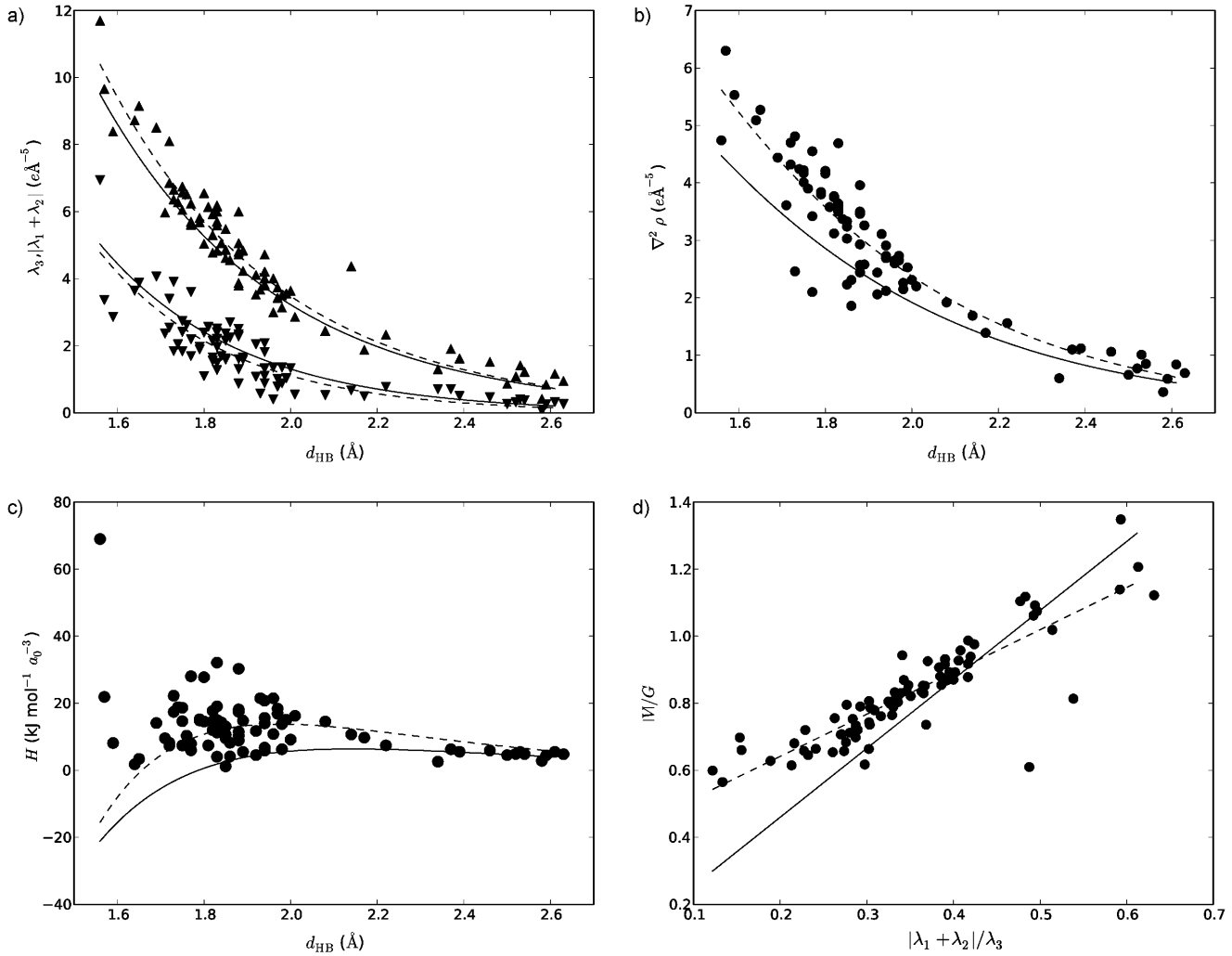

Figure 5. a) λ_3 (▲) and $|\lambda_1 + \lambda_2|$ (▼) versus d_{HB}, b) $\nabla^2\rho$ versus d_{HB}, c) H versus d_{HB} and d) $|V|/G$ versus $|\lambda_1 + \lambda_2|/\lambda_3$ for the experimental H···O data from reference [18]. Solid and dashed lines are obtained from the linear regressions calculated with theoretical and experimental data (column X=O (exp) in Table 2), respectively.

correspondence between the experimental data and the theoretical dependency unclear. This feature is similar to what happens with the dependencies between the topological and the energetic properties. In this last case, parameters are close enough as to assume that theoretical dependencies reproduce well the experimental behaviour, with the only exception of $|V|/G$ versus $|\lambda_1 + \lambda_2|/\lambda_3$ (Figure 5 d).

Dispersion of values around the expected dependencies is much larger for the experimental than for the theoretical data, as indicated by the larger RMSD and NRMSD and the systematically lower R^2 values in the experimental case. This dispersion is commonly attributed to observational errors, which are related to the difference between the experimentally determined and the true magnitude of $\rho(\mathbf{r})$. In that case, a good estimation of the $\rho(\mathbf{r})$ properties at the BCP can be obtained from the fitting functions build either from experimental data[18] or from the theoretical dependencies presented here, provided that an accurate set of atomic coordinates, including those of hydrogen atoms, is available. However, it must be noted that while theoretical data comes from complexes in the gas phase formed by two molecules joined by a single hydrogen bond, experimental data comes from interactions between molecules that are usually involved in several intermolecular interactions and embedded in a crystal environment. Thus, it should not be excluded that HB cooperativity or the electric field generated by the surrounding molecules play a significant role in the larger dispersion observed in the experimental case, to the point that information about the effect of the environment on the interaction could be retrieved from the topology of the experimental $\rho(\mathbf{r})$.

While further research will be undertaken to elucidate this last issue, the dependencies pointed out for the theoretically calculated $\rho(\mathbf{r})$ properties at the BCP can be used in the analysis of experimental electron densities. This can be useful when dealing with complicated situations in the determination of crystalline $\rho(\mathbf{r})$, as for example in the case of large systems or when problems in the modelling of experi-

mental data appear.[35] Outliers or systematic deviations from the expected dependencies should be regarded with special care, as they could be indicative of errors in the determination of $\rho(\mathbf{r})$ or of uncommon features in $\rho(\mathbf{r})$ that should be analyzed in detail.

Conclusion

The theoretical analysis of a large set of H···X hydrogen bonded complexes reveals that hydrogen bonds can be classified in families according to the acceptor entity X, which can be an atom or a π orbital. Each family is characterised by a set of dependencies between the electron properties at the H···X bond critical point, as well as between them and the hydrogen bond distance d_{HB}. For X = H, C, N, O, F, S or Cl, the dependencies with the bonding distance observed for the electron density, the curvatures and the electron kinetic and potential energy densities at the BCP appear classified according to the van der Waals radius r_X of the acceptor atom. Other dependencies, as for example that of the Laplacian with the hydrogen-bond distance, or the linear relationships between the curvatures and the local energy densities, exhibit a classification along series of acceptors belonging to the same row of the periodic table. These orderings can be explained in terms of the penetration of the electron shells of the H···X interacting atoms and on the effect of the acceptor atom electronegativity, which influences the balance between the closed shell/shared character of the interaction. Thus, as more electronegative is the acceptor atom, the interaction tends to be more of closed shell type and significant shared character is therefore restricted to shorter bonding distances, indicating that the hydrogen bond is more polarised and less charge is accumulated in the internuclear region for a larger domain of H···X distances. Similarly, as the van der Waals radius increases, the concentration of electrons is favoured, therefore leading to a higher degree of shared type. Thus, pure closed-shell interactions are abandoned at larger distances with higher r_X values.

Among the analysed hydrogen-bonding interactions, H···π deserves a particular consideration. Indeed, in spite the functional dependencies of the $\rho(\mathbf{r})$ properties at the BCP are entirely similar for H···π and H···X (X = H, C, N, O, F, S or Cl) families, the fitting functions obtained for the former cross those corresponding to the latter. This feature indicates that even if the qualitative behaviour of the H···π interaction can be brought close to that of H···X, it can not be classified within the latter group, pointing to a particular specificity for H···π interactions.

The electron properties at the H···X BCP (X = H, C, N, O, F, S, Cl, π) can be determined, to a first approximation, by the hydrogen-bond distance at equilibrium, which in turn is fixed by the chemical environment of the interaction. At the same time, the specific environment around the H···X region of each complex also induces a dispersion of values around the expected dependencies, being more pronounced for some properties than for others.

The theoretical results obtained in this work validate the empirical dependencies derived from experimental high-resolution X-ray diffraction data, as shown by the good agreement between both the experimental and the theoretical dependencies determined for H···O hydrogen bonds, in spite of a much larger dispersion of values observed in the experimental case. To which extent this larger dispersion is due to experimental errors or to the complex effect of the crystal environment is an important issue that should be investigated in order to know which information corresponding to the molecular environment effect on the hydrogen-bond interaction can be retrieved from the experimental electron density. As there is no reason why a similar behaviour should not be present in the other families, the dependencies between the electron properties at the BCP, as well as between them and the bonding distance, for all kind of hydrogen bonds can be used in the analysis of experimental electron densities. Thus, while it is expected that properties at the BCP from experimental electron densities should fall close to the expected dependencies, large deviations should be taken as indicative of either errors in the model or uncommon features worth of a more in-deep analysis.

Computational Methods

Calculations were performed on a large set of 163 complexes formed by a pair of donor (FH, NCH, CHN, ClH or HCCH) and acceptor molecules (see Supporting Information for a complete list of the calculated complexes) joined by a single H···X hydrogen bond (X = H, C, N, O, F, S, Cl or π, depending on the acceptor molecule). The distribution of the complexes according to X is given in Table 1. Their geometries were fully optimised at the MP2/6-311++G(d,p) computational level (X = C, O, S, Cl and π) or taken from previous publications[22,23,36] for X = F, N and H, respectively). In all cases, the topological analysis was performed on a $\rho(\mathbf{r})$ function calculated at MP2/6-311++G(d,p) level of theory, after checking by frequency calculations that the geometry corresponded to a minimum of energy. Gaussian-03[37] and AIMPAC[38] programs were used for the theoretical calculations and the topological analysis, respectively. A complete list of complexes and HB critical point properties is given in Supporting Information.

A set of 12 dependencies was calculated for each one of the eight families of complexes having the same acceptor X. In order to compare with the theoretical data, a similar set of dependencies was also calculated for the 83 experimentally determined H···O hydrogen bonds taken from reference [18]. Three kinds of dependencies were considered: exponential ($y(x) = ae^{-bx}$), power ($y(x) = ax^b$) and linear ($y(x) = a + bx$). While exponentials were used for the dependencies of BCP properties with d_{HB},[39] linear functions were used for the energy densities and ρ dependencies with the curvatures. The power form was preferred to the exponential function $y(x) = a(1-e^{bx})$, previously reported for $|\lambda_1 + \lambda_2|$ versus λ_3 and $|V|$ versus G,[19] as this is the expected dependency between two properties that decay exponentially with d_{HB}. For X = π, the bond path connects the hydrogen nucleus with the BCP of the chemical bond to which the π orbital is involved. In this case, d_{HB} has been taken as the distance from this BCP to the hydrogen atom.

Exponential and power dependencies were linearised by using logarithms. The a and b fitting parameters were then calculated by linear regressions.[40] Results are reported in Table 2, where a and b are listed together with R^2, RMSD and normalised RMSD (NRMSD) values, the latter defined as the RMSD divided by the range of values of the dependent property (RMSD/($y_{max} - y_{min}$)). This method was preferred to the least squares fitting of an exponential or power function because it

avoids the bias toward large values that appears in this last case. For comparison, the dependencies were also calculated from least squares fits against the original data. These results are not however reported here because they are mostly similar to those from linear regressions on linearised data. The few significant differences are explained in the results and discussion section.

Acknowledgements

The authors are grateful to Prof. Richard F. W. Bader for helpful comments. This work was supported by the Spanish Ministerio de Educación y Ciencia (MEC) (Grant Nos. MAT2006-13572-C02-01, CTQ2007-61901/BQU and CONSOLIDER CSD2007-00041) and Generalitat de Catalunya (Grant No. 2005SGR-452), I.M. also thanks MEC for a Juan de la Cierva fellowship.

[1] R. F. W. Bader, *Atoms in Molecules: A Quantum Theory*, Clarendon, Oxford, **1990**.
[2] *The Quantum Theory of Atoms in Molecules: From Solid State to DNA and Drug Design* (Eds.: C. F. Matta, R. J. Boyd), Wiley-VCH, Weinheim, **2007**.
[3] R. F. W. Bader, *J. Phys. Chem. A* **1998**, *102*, 7314–7323.
[4] R. F. W. Bader, *Phys. Rev. B* **1994**, *49*, 13348–13356.
[5] W. J. Hehre, L. Radom, P. V. R. Schleyer, J. Pople, *Ab Initio Molecular Orbital Theory*, Wiley, New York, **1986**.
[6] P. Coppens, *X-Ray Charge Densities and Chemical Bonding*, Oxford University Press, Oxford, **1997**.
[7] Yu. A. Abramov, *Acta Crystallogr. Sect. A* **1997**, *53*, 264–272.
[8] N. H. March, *Adv. Phys.* **1957**, *6*, 1–101.
[9] C. F. von Weizsacker, *Z. Phys.* **1935**, *96*, 431–458.
[10] D. A. Kirzhnitz, *Sov. Phys. JETP* **1957**, *5*, 64–72.
[11] R. F. W. Bader, *J. Chem. Phys.* **1980**, *73*, 2871–2883.
[12] E. Espinosa, E. Molins, C. Lecomte, *Chem. Phys. Lett.* **1998**, *285*, 170–173.
[13] E. Espinosa, I. Alkorta, I. Rozas, J. Elguero, E. Molins, *Chem. Phys. Lett.* **2001**, *336*, 457–461.
[14] R. J. Boyd, S. C. Choi, *Chem. Phys. Lett.* **1985**, *120*, 80–85.
[15] O. Knop, R. J. Boyd, S. C. Choi, *J. Am. Chem. Soc.* **1988**, *110*, 7299–7301.
[16] O. Knop, K. N. Rankin, R. J. Boyd, *J. Phys. Chem. A* **2001**, *105*, 6552–6566.
[17] O. Knop, K. N. Rankin, R. J. Boyd, *J. Phys. Chem. A* **2003**, *107*, 272–284.
[18] E. Espinosa, M. Souhassou, H. Lachekar, C. Lecomte, *Acta Crystallogr. Sect. B* **1999**, *55*, 563–572.
[19] E. Espinosa, C. Lecomte, E. Molins, *Chem. Phys. Lett.* **1999**, *300*, 745–748.
[20] P. M. Dominiak, A. Makal, P. R. Mallinson, K. Trzcinska, J. Eilmes, E. Grech, M. Chruszcz, W. Minor, K. Wozniak, *Chem. Eur. J.* **2006**, *12*, 1941–1949.
[21] M. V. Vener, A. V. Manaev, A. N. Egorova, V. G. Tsirelson, *J. Phys. Chem. A* **2007**, *111*, 1155–1162.
[22] E. Espinosa. I. Alkorta, J. Elguero, E. Molins, *J. Chem. Phys.* **2002**, *117*, 5529–5542.
[23] I. Mata, E. Molins, I. Alkorta, E. Espinosa, *J. Phys. Chem. A* **2007**, *111*, 6425–6433.
[24] A. Costales, M. A. Blanco, A. Martín Pendás, P. Mori-Sanchez, V. Luaña, *J. Phys. Chem. A* **2004**, *108*, 2794–2801.
[25] T. B. Richardson, S. de Gala, R. H. Crabtree, *J. Am. Chem. Soc.* **1995**, *117*, 12875–12876.
[26] C. F. Matta, J. Hernández-Trujillo, T.-H. Tang, R. F. W. Bader, *Chem. Eur. J.* **2003**, *9*, 1940–1951.
[27] A. Bondi, *J. Chem. Phys.* **1964**, *40–41*, 441–451.
[28] M. T. Carroll, R. F. W. Bader, *Mol. Phys.* **1988**, *65*, 695–722.
[29] O. Galvez, P. C. Gómez, L. F. Pacios, *J. Chem. Phys.* **2009**, *130–131*, 11166–11184.
[30] I. Mata, E. Molins, I. Alkorta, E. Espinosa, *J. Chem. Phys.* **2009**, *130*, 044104.
[31] A. H. Pakiari, S. Fakhraee, *J. Theor. Comput. Chem.* **2006**, *5*, 621–631.
[32] G. Gervasio, R. Bianchi, D. Marabello, *Chem. Phys. Lett.* **2004**, *387*, 481–484.
[33] P. Macchi, A. Sironi, *Coord. Chem. Rev.* **2003**, *238–239*, 383–412.
[34] E. Espinosa, I. Alkorta, I. Mata, E. Molins, *J. Phys. Chem. A* **2005**, *109*, 6532–6539.
[35] I. Mata, E. Espinosa, E. Molins, S. Veintemillas, W. Maniukiewicz, C. Lecomte, A. Cousson, W. Paulus, *Acta Crystallogr. Sect. A* **2006**, *62*, 365–378.
[36] I. Alkorta, K. Zborowski, J. Elguero, M. Solimannejad, *J. Phys. Chem. A* **2006**, *110*, 10279–10286.
[37] Gaussian 03, Revision E.01, M. J. Frisch, G. W. Trucks, H. B. Schlegel, G. E. Scuseria, M. A. Robb, J. R. Cheeseman, J. A. Montgomery, Jr., T. Vreven, K. N. Kudin, J. C. Burant, J. M. Millam, S. S. Iyengar, J. Tomasi, V. Barone, B. Mennucci, M. Cossi, G. Scalmani, N. Rega, G. A. Petersson, H. Nakatsuji, M. Hada, M. Ehara, K. Toyota, R. Fukuda, J. Hasegawa, M. Ishida, T. Nakajima, Y. Honda, O. Kitao, H. Nakai, M. Klene, X. Li, J. E. Knox, H. P. Hratchian, J. B. Cross, V. Bakken, C. Adamo, J. Jaramillo, R. Gomperts, R. E. Stratmann, O. Yazyev, A. J. Austin, R. Cammi, C. Pomelli, J. W. Ochterski, P. Y. Ayala, K. Morokuma, G. A. Voth, P. Salvador, J. J. Dannenberg, V. G. Zakrzewski, S. Dapprich, A. D. Daniels, M. C. Strain, O. Farkas, D. K. Malick, A. D. Rabuck, K. Raghavachari, J. B. Foresman, J. V. Ortiz, Q. Cui, A. G. Baboul, S. Clifford, J. Cioslowski, B. B. Stefanov, G. Liu, A. Liashenko, P. Piskorz, I. Komaromi, R. L. Martin, D. J. Fox, T. Keith, M. A. Al-Laham, C. Y. Peng, A. Nanayakkara, M. Challacombe, P. M. W. Gill, B. Johnson, W. Chen, M. W. Wong, C. Gonzalez, J. A. Pople, Gaussian Inc., Wallingford, CT, **2004**.
[38] F. Biegler-König, R. Bader, T.-H. Tang, *J. Comput. Chem.* **1982**, *3*, 317–328.
[39] I. Alkorta, L. Barrios, I. Rozas, J. Elguero, *J. Mol. Struct.* **2000**, *516–558*, 131–137.
[40] I. Alkorta, J. Elguero, *J. Phys. Chem. A* **1999**, *103*, 272–279.

Received: June 15, 2009
Published online: January 14, 2010

